ACS APPLIED MATERIALS & INTERFACES

Research Article

www.acsami.org

Flexible Polyimide Films Hybrid with Functionalized Boron Nitride and Graphene Oxide Simultaneously To Improve Thermal Conduction and Dimensional Stability

Mei-Hui Tsai,[†] I-Hsiang Tseng,*[,‡] Jen-Chi Chiang,[†] and Jheng-Jia Li[†]

[†]Department of Chemical and Materials Engineering, National Chin-Yi University of Technology, No. 57, Sec. 2, Chungshan Road, Taipin District, Taichung 41170, Taiwan

[‡]Department of Chemical Engineering, Feng Chia University, No. 100, Wenhwa Road, Seatwen District, Taichung 40724, Taiwan

ABSTRACT: Coupling agent-functionalized boron nitride (f-BN) and glycidyl methacrylate-grafted graphene (g-TrG) are simultaneously blended with polyimide (PI) to fabricate a flexible, electrically insulating and thermally conductive PI composite film. The silk-like g-TrG successfully fills in the gap between PI and f-BN to complete the thermal conduction network. In addition, the strong interaction between surface functional groups on f-BN and g-TrG contributes to the effective phonon transfer in the PI matrix. The thermal conductivity (TC) of the PI/f-BN composite films containing additional 1 wt % of g-TrG is at least doubled to the value of PI/f-BN and as high as 16 times to that of the pure PI. The hybrid film PI/f-BN-50/g-TrG-1 exhibits excellent flexibility, sufficient insulating property, the highest TC of 2.11 W/mK, and ultralow coefficient of thermal expansion of 11 ppm/K, which are perfect conditions for future flexible substrate materials requiring efficient heat dissipation.

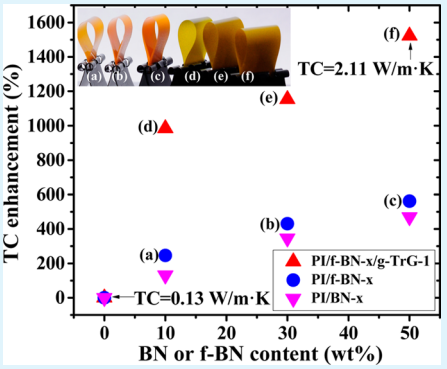

KEYWORDS: *thermal conductivity, graphene oxide, boron nitride, polyimide, dimensional stability*

1. INTRODUCTION

Polyimide (PI)-based substrates are potential materials in advanced electronic systems, such as flexible printed circuits (FPC) and flexible displays, due to the requirement of flexibility, lightweight, and robustness.[1−4] However, the increased power density in advanced electronics makes effective heat removal a critical concern for a reliable performance. Different types of thermally conductive fillers have been incorporated with polymer matrices to improve the thermal conductivity (TC) of the resultant polymer composites.[5−9] However, the thermal resistance at the interface between filler and polymer is created and should be minimized to facilitate smooth heat transfer in polymer composites.[6,9−11] Another prominent factor to facilitate efficient phonon transfer or lattice vibration in polymer matrix is to form a thermally conductive network by appropriate selection and packing of conductive fillers in polymer matrix.[9,12,13] Introduction of fillers with high aspect ratios[5,10] or a hybrid filler system[7,10,14,15] in polymer matrix allows the formation of a conducting network for thermal energy. However, a large contact area between filler and polymer might increase the resistance of heat transport at the interface.[11] Hence, the affinity of filler to polymer should also be improved by modifying the surface of fillers.[9,16] The functional groups on fillers will assist the movement of phonon between the thermally conductive filler and the polymer matrix,[11] and consequently the efficiency of heat transportation in polymer matrix can be increased.

For the electronic applications, the thermally conductive but electrically insulating PI composites are essential.[6,9,12,17−19] Therefore, highly electrical conductive materials, such as carbon nanotubes, are not appropriate fillers for thermally conductive PI in electronic devices. Other candidate fillers, including aluminum nitride (AlN) and boron nitride (BN), have been blended with polymer matrix. Xie et al. prepared a thermally conductive PI composite containing 32 vol % modified AlN, and its thermal conductivity (TC) reaches 0.8 W/mK, compared to 0.22 W/mK for pure PI.[7] Li and Hsu[12] prepared a PI composite containing 30 wt % of surface-modified micro- and nanosized BN fillers with an enhanced TC up to 1.2 W/mK. For electronic applications, a lower water absorption rate of the polymer substrate is essential. Consequently, a more hydrophobic BN is superior to AlN as the filler in those polymer substrates.[9] In addition, the packing density of BN in polymer is much higher than that of other fillers that the filler content in polymer matrix can be decreased.[6] Hence, the insulating and lubricating BN was considered the candidate filler for thermally conductive PI films for electronic usage. On the other hand, graphene-related nanofillers have been confirmed as efficient thermal interface materials to minimize the thermal resistance between two surfaces.[20] Although graphene nanosheets are excellent materials for both thermal and electrical conductivity,[21] the electrical conductivity of the chemically converted graphene, i.e. graphene oxide (GO), is not as high as

Received: March 12, 2014
Accepted: May 15, 2014
Published: May 27, 2014

   dx.doi.org/10.1021/am501323m | ACS Appl. Mater. Interfaces 2014, 6, 8639−8645

that of the pristine graphene or carbon nanotube (CNT) due to the retained oxygen-related groups.[22−24]

Previously, we have investigated the effects of single filler, BN or chemically exfoliated GO, contents on the TCs of PI films. With the blending of 50 wt % coupling agent-modified BN fillers, the TC value of PI composite is 0.86 W/mK, compared with 0.13 W/mK for pure PI.[25] On the other hand, the PI composite film containing 10 wt % of surface-modified GO (g-GO) has a TC up to 0.81 W/mK,[26] which is a compatible enhancement in TC for the PI containing 50 wt % of BN. The microsized BN platelets and thermally reduced GO (TrG) nanosheets were reacted with PI in order to complete the conductive network in the electrically insulating PI matrix. The dimensional stability, TC, and mechanical strength of PI hybrid films were correlated with the type and composition of thermally conductive fillers. By appropriate selection and packing of functionalized BN (f-BN) and grafted TrG (g-TrG) in the PI matrix, the PI hybrid films have the potential in modern electronic devices requiring efficient heat transportation and superior thermal stability.

2. EXPERIMENTAL SECTION

2.1. Materials. Pyromellitic dianhydride (PMDA) and 4,4′-diaminodiphenyl ether (ODA) were purchased from Aldrich (USA). Anhydrous dimethylacetamide (DMAc), *N*-methyl-2-pyrrolidone (NMP), and the thermal initiator 2,2′-azobis-isobutyronitrile (AIBN) were provided by Showa Chemical Co. (Japan). Glycidyl methacrylate (GMA, 99.5%) from Aldrich (USA) from Acros (USA) was employed as-received. Natural graphite powder (325 mesh) was supplied by Alfa-Aesar (USA). Hexagonal BN nanosheets with the purity of 99.0%, the mean size of 4 μm (NW-04) or 15 μm (SW-15), and the specific surface area of 11 m^2/g (NW-04) or 13 m^2/g (SW-15) were courtesy of National Nitride Technologies Co. (Taiwan). The titanate coupling agent (KR-44) from TCI with the chemical structure shown in Figure 1 was employed to modify the surface of BN.

2.2. Functionalization of BN. BN platelets with the mean particle size of 4 or 15 μm were dispersed in solvent DMAc and ultrasonic for 2 h at room temperature. The coupling agent KR-44 with the weight ratio of 0.01 to BN was mixed with the above suspensions dropwise and continue stirred at 80 °C for 24 h to complete the sol−gel process between the hydroxyl groups on BN and the amine group on KR-44. The f-BN was then obtained after washing, centrifuging, and drying treatments.

2.3. Preparation and Functionalization of Graphene Oxide. GO was chemically exfoliated from graphite by the modified Hummers method[26] and followed by the centrifugation and vacuum-drying at 60 °C. The dried GO was then placed under heat treatment at a heating rate of 2 °C/min to 1050 °C to obtain TrG nanosheets. TrG and AIBN were dispersed in NMP and ultrasonificated at 65 °C for 2 h followed by the addition of GMA at a fixed weight ratio of 1:0.5:0.03 for TrG:AIBN:GMA. The mixture was continuously stirred at 80 °C for 24 h under N_2 to accomplish the grafting of GMA on TrG.[27] The resultant GMA-grafted TrG slurry was washed and centrifuged several times with acetone to remove the free GMA molecule or its oligomers. The precipitates were collected and then dried in a vacuum oven to obtain g-TrG.

2.4. Preparation of PI/f-BN/g-TrG Composite Films. The synthesize procedure of PI/f-BN/g-TrG films is shown in Figure 1. Typically, ODA (10 mmol) was thoroughly dissolved in DMAc in a three-necked flask equipped with a mechanical stirrer at room temperature under N_2. PMDA (9 mmol) was sequentially mixed with the above ODA solution every 0.5 h to obtain a viscous poly(amic acid) (PAA) solution with a chain length of 5000 g/mol. Two types of f-BN platelets with mean particle sizes of 15 and 4 μm were selected and mixed with the weight ratio of 70% and 30%. The size-mixed f-BN and g-TrG were dispersed in DMAc with the assistance of ultrasonic vibration prior to the mixing with the above PAA solution. The final portion of PMDA (1 mmol) was mixed and continuously stirred at room

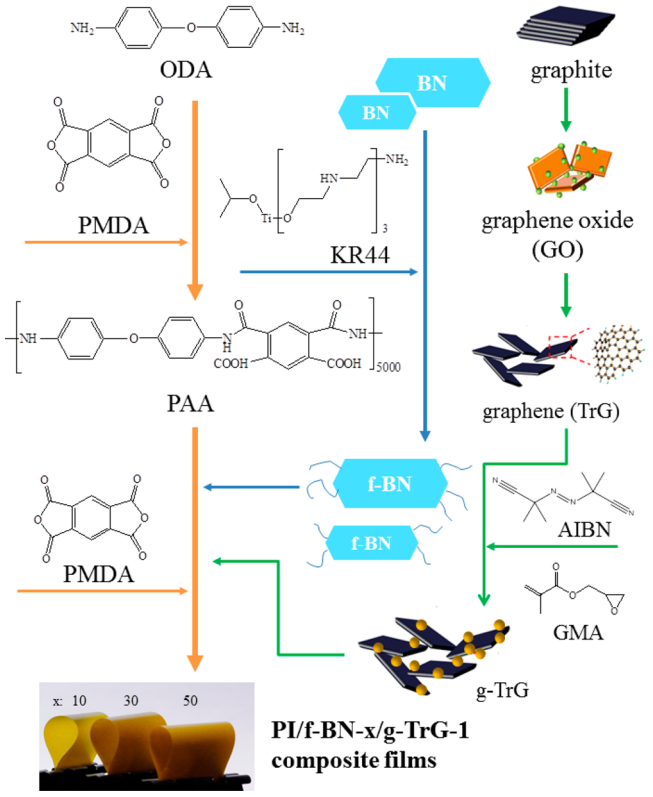

Figure 1. Procedure of preparing fillers (f-BN and g-TrG) and composite films (PI/f-BN-x/g-TrG-1).

temperature for 6 h to obtain a homogeneous viscous PAA/f-BN/g-TrG solution. The above solution was cast on a glass substrate by a scalpel and transformed to the PI/f-BN/g-TrG film after the following thermal imidization process. The casted film was imidized in an oven at a heating rate of 2 °C/min, from 80 °C through 150 and 170 °C, annealing at each temperature for 1 h, and finally to 350 °C and annealing for 2 h. The thickness of the resultant PI/f-BN/g-TrG film was about 20 μm. The sample code was denoted PI/f-BN-x/g-TrG-y, where x and y represent the wt % of f-BN and g-TrG, respectively, in PI composites. In this study, x was ranging from 10 to 50 and y was fixed to 1. The same procedure was applied to synthesize PI/f-BN-x, PI/BN-x, or PI/g-TrG-y films containing single type of filler f-BN, BN, or g-TrG. In addition, a reference PI film without the addition of those fillers was also synthesized and denoted pure PI. The digital photos of flexible PI/f-BN/g-TrG composite films are shown in Figure 1.

2.5. Characterizations. The morphology of BN, TrG, g-TrG, and PI composites were investigated by the transmission electron microscopy (TEM) and scanning electron microscopy (SEM) using electron microscopes JEOL TEM-2100 and JEOL SEM-6700F, respectively. For TEM measurements, samples were prepared by drop casting on carbon-coated copper grids followed by solvent evaporation in air at room temperature. Infrared spectra of PAA solution at various temperatures were obtained to identify the imidization degree by using a Nicolet Protégé-460 Fourier transform infrared (FTIR) spectrophotometer equipped with a variable-temperature sample holder. Thermogravimetric analysis (TGA) was performed using a TGA analyzer (Q500, TA Instrument) at a heating rate of 10 °C/min under N_2. The temperature at 5 wt % weight loss was denoted the thermal decomposition temperature (T_d^5) in this work. The storage modulus and tan δ were measured using a dynamic mechanical analyzer (DMA, 2980, TA Instrument) at a heating rate of 3 °C/min. The glass transition temperature (Tg) was determined from the peak temperature of tan δ curve. The thermal mechanical analyzer (TMA, Q400, TA Instrument) was conducted under an extension mode, with a tension force of 0.05 N, at a heating rate of 10 °C/min, at a frequency of 1 Hz, and under N_2. The coefficient of thermal expansion (CTE) was evaluated from the TMA

data in the temperature range of 100 to 200 °C, which is a commonly testing condition in manufacturing. The crystalline structures of nanofillers and deposited films were identified by X-ray diffraction (XRD) using a Shimadzu XRD-6000 equipped with a CuKα radiation (λ = 0.154 nm) at 40 kV and 30 mA. An X-ray photoelectron spectroscopy (XPS) (ESCA PHI-1600, Physical Electronics) was utilized to detect the surface composition of nanofillers. The TC of films (diameter: 20 mm) at room temperature and at a fixed load of 20 kgf was measured on a TC tester (CL-TIM from Taiwan) based on the ASTM D-5470 standard. Thermal-conductive grease (TC-5121 from Dow Corning) was applied on both sides of each specimen to reduce the thermal resistance at the interface between copper and sample. The surface resistance (Rs) of each film (sample size: 10 cm square) at room temperature was measured on a megaohm-meter (Hioki SME-8310) at a DC voltage of 100 V. The TC and Rs values presented in this work are the average values of at least three measurements of each sample.

3. RESULTS AND DISCUSSION

3.1. Characteristics of Functionalized Fillers. The FTIR spectra of dried BN and f-BN platelets are shown in Figure 2. The

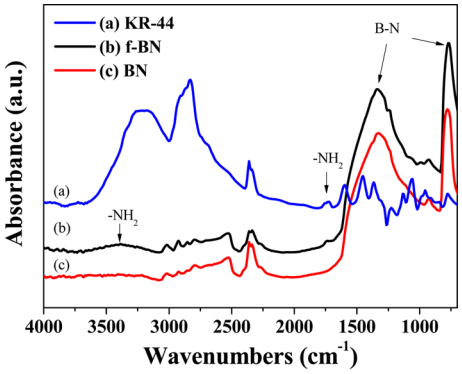

Figure 2. FTIR spectra of (a) Ti-coupling agent (KR-44), (b) Ti-coupling agent-functionalized boron nitride (f-BN), and (c) dried boron nitride (BN).

characteristic B−N stretch and bending peaks[12,16] around 1381 and 791 cm^{-1} were observed from BN platelets before and after surface modification. The B-NH_2 or B−OH stretching vibrations[9] on the BN surface were not significant on the FTIR spectra of BN. The absorption peak of amine groups at 1730 cm^{-1} were observed from both f-BN and Ti-coupling agent KR44 indicating the presence of KR44 on f-BN.

In order to further confirm the successful modification of f-BN, the XPS spectra of BN and f-BN are compared. As shown in Figure 3, the additional Ti 2p signals presented in the survey XPS

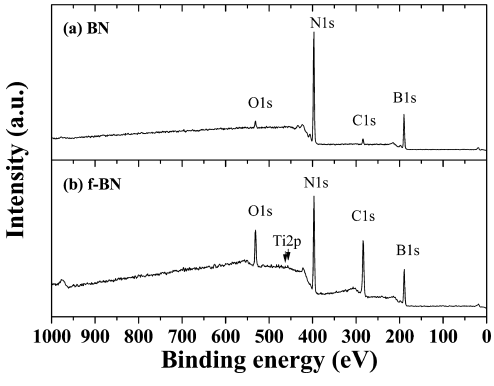

Figure 3. XPS full-scan spectra of (a) BN and (b) f-BN.

spectra of f-BN. The XPS (Ti 2p) spectrum of f-BN (Figure 4) exhibits the characteristic Ti−O binding energy at 458.2 and

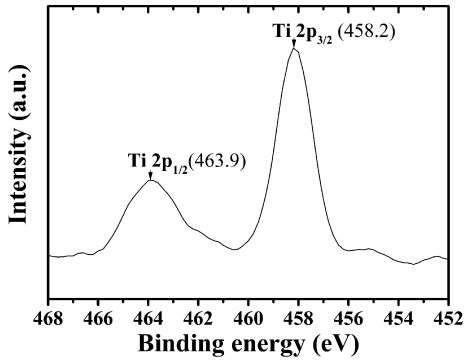

Figure 4. XPS Ti 2p spectrum of f-BN.

463.9 eV.[28] The existence of C and O in BN platelets is consistent with the literature.[29] The atomic ratios of O and C on f-BN increase to 8.6 and 31.4%, respectively, compared to 2.4 and 4.1% for pure BN. The increase in Ti, C, and O amounts on f-BN suggests the successful modification of BN by the Ti-coupling agent KR-44. There is no significant difference in XPS B 1s and N 1s spectra between BN and f-BN. The dominant B 1s peak centered at 190.3 eV and the N 1s peak at 397.9 eV for both BN samples are the characteristic binding energies of hexagonal BN.[30]

The XRD patterns of obtained TrG nanosheets together with the precursor graphite and GO are displayed in Figure 5(a-c).

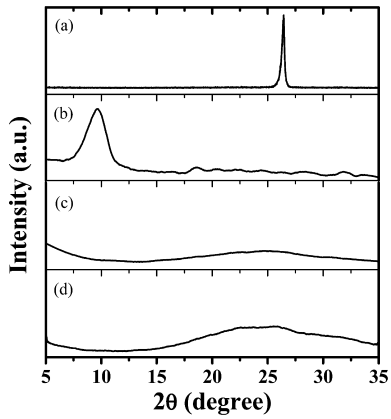

Figure 5. XRD patterns of (a) graphite, (b) GO, (c) TrG, and (d) g-TrG.

The XRD pattern of natural graphite reveals the characteristic intense diffraction peak of graphite at 2θ = 26.4°, which corresponds to the graphene interlayer of (002) with the d spacing of 0.34 nm.[31−33] The disappearance of the characteristic graphite peak at 26.4° and the formation of a broad peak at 9.7° (d = 0.92 nm) of dried GO indicate the intercalation of hydroxyl, carbonyl, and epoxide groups in graphite interlayer during the chemical oxidation process.[31,32,34] Abundant amounts of those functional groups on the surface of GO were removed and simultaneously leading to a fast exfoliation during the thermal treatment to obtain RG as confirmed in the following XPS results. The absence of significant diffraction peak in the XRD pattern of TrG reveals the exfoliated feature after the thermal reduction of GO. The interlayer distance of TrG remains during

dx.doi.org/10.1021/am501323m | ACS Appl. Mater. Interfaces 2014, 6, 8639−8645

the GMA-modification process because the similar XRD patterns were obtained from g-TrG and TrG.

The TGA curves of graphite, GO, TrG, and g-TrG are shown in Figure 6. Two weight loss stages are observed for GO sample.

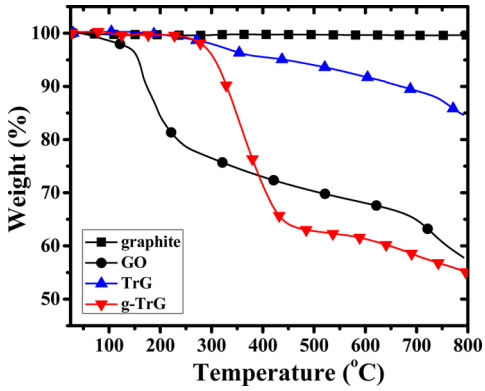

Figure 6. TGA curves of graphite, GO, TrG, and g-TrG.

The first weight loss stage below 250 °C is due to the decomposition of surface carboxyl or hydroxyl groups on GO.[27,35] For the thermally reduced TrG sample, the weight loss below 250 °C is negligible indicating the successful removal of the oxygen-related functional groups during the heat treatment. Some oxygen-containing functional groups remain on TrG as evidenced in XPS data that around 5 wt % of weight loss of TrG is obtained in the temperature range of 250 to 450 °C. For g-TrG, the weight loss starting from 300 to 450 °C resulted from decomposition of the grafted polymers on TrG.[27] Based on the percentage of weight loss, the grafted polymer on TrG is around 35 wt % of TrG, corresponding to a grafting ratio of 70% of introduced GMA precursor.

The surface composition of TrG is examined and compared to that of g-TrG by the analysis of their XPS spectra. Figure 7 (a) illustrates the raw data and deconvoluted XPS spectra in the C 1s region of TrG. The graphitic C═C and C−C structures are revealed at the binding energy of 284.2 and 284.7 eV, respectively.[33,36,37] Compared with the XPS results of GO, the intensity of graphitic C═C components on TrG increased indicating the successful thermal reduction of TrG from GO. In addition, the splitting of the C 1s peak at higher binding energy for TrG is negligible. The results suggest few oxidized carbon functional groups including C−OH (286.5 eV), C−O−C (286.8 eV), C═O (287.3 eV), and O−C═O (288.6 eV)[33,37,38] remained on TrG after the thermal treatment on GO. In contrast, the oxygen-containing functional groups appear on g-TrG. The deconvoluted XPS curves show an increased epoxy signal at 286.5 eV on g-TrG indicating the successfully grafting of GMA on TrG.

The morphology of fillers is shown in Figure 8. The TEM image of TrG demonstrates ultrathin sheets with wrinkled, folded, and silk-like morphology as shown in Figure 8(a). We also observed an ordered and layered lattice structure of carbons at the edges or the folding of the graphene nanosheets from a high-magnified image as shown in Figure 8(b). The number of graphene layers is around 22 layers with the thickness of 8 nm. The dark spots, which are believed to be the polymerized GMA,[27,38] are distributed on the surface of TrG as displayed in Figure 8(c). The SEM images shown in Figure 8(d, e) demonstrate the distribution of individual f-BN (30 wt %) or g-TrG (1 wt %), respectively, in PI composites. The improved

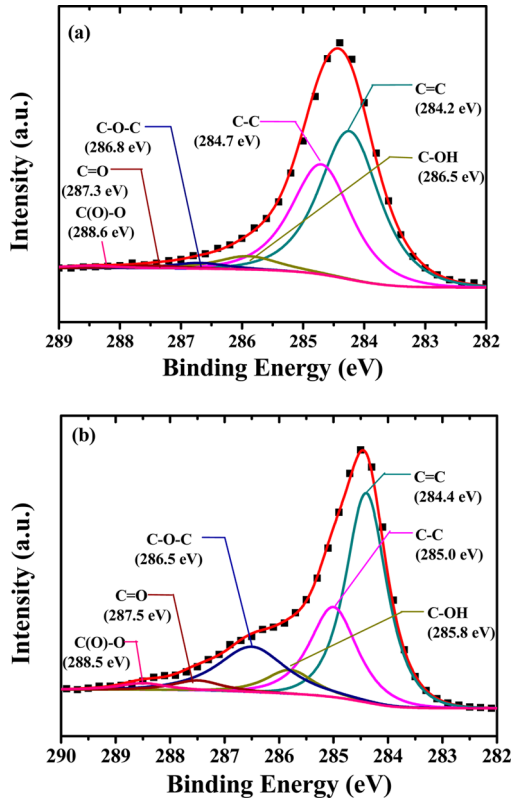

Figure 7. XPS C 1s spectra and deconvolution results of (a) TrG and (b) g-TrG.

compatibility between two phases resulted in the appropriate surface modification of BN and TrG. The distribution of hybrid fillers in the PI matrix can be examined from Figure 8 (f, g). Similar plastic deformation features are observed from the fractured surface of the PI/f-BN-30/g-TrG-1 composite film suggesting the strong interactions between PI and fillers. More importantly, the wrinkled g-TrG is attached closely to the edge of f-BN and perfectly filled the gap between PI and f-BN. The strong interaction comes from the reactivity of those functional groups, amine and epoxy, respectively, on f-BN and g-TrG. The epoxy groups on g-TrG also lead to better compatibility of TrG to the PI matrix as confirmed by previous study.[26] Consequently, the enhanced affinity of nanofillers to the PI matrix is responsible for the improvement of the thermal and mechanical properties of the resultant PI composite films.

3.2. Improved Properties of PI Composites by Hybrid Filler System. Based on previous results,[25,26] the optimum combination of two-size-mixed BN platelets is determined to be 30 wt % of 4 μm and 70 wt % of 15 μm to efficiently improve the TC of the PI/BN composite films. In addition, the effect of total BN contents on the TC value of the PI films is evaluated in this study. As shown in Figure 9(a), the TC value of the PI film containing hybrid BN platelets asymptotically increases from 0.13 W/mK (for pure PI) to 0.74 W/mK (for PI/BN-50). The improvement of TC by the surface modification of BN is limited as shown by the TC value of PI/f-BN-50 only slightly increases to 0.86 W/mK. On the other hand, a significant enhancement in TC is observed for PI films containing only 1 wt % of g-TrG (the star legend in Figure 9(a)). The TC value of PI/g-TrG-1 is as high as 0.41 W/mK, which is comparable to that of PI/f-BN-10. The additional 1 wt % g-TrG in the PI/f-BN-50 matrix dramatically increases the TC value by a factor of 3, accordingly from 0.74 to

dx.doi.org/10.1021/am501323m | ACS Appl. Mater. Interfaces 2014, 6, 8639−8645

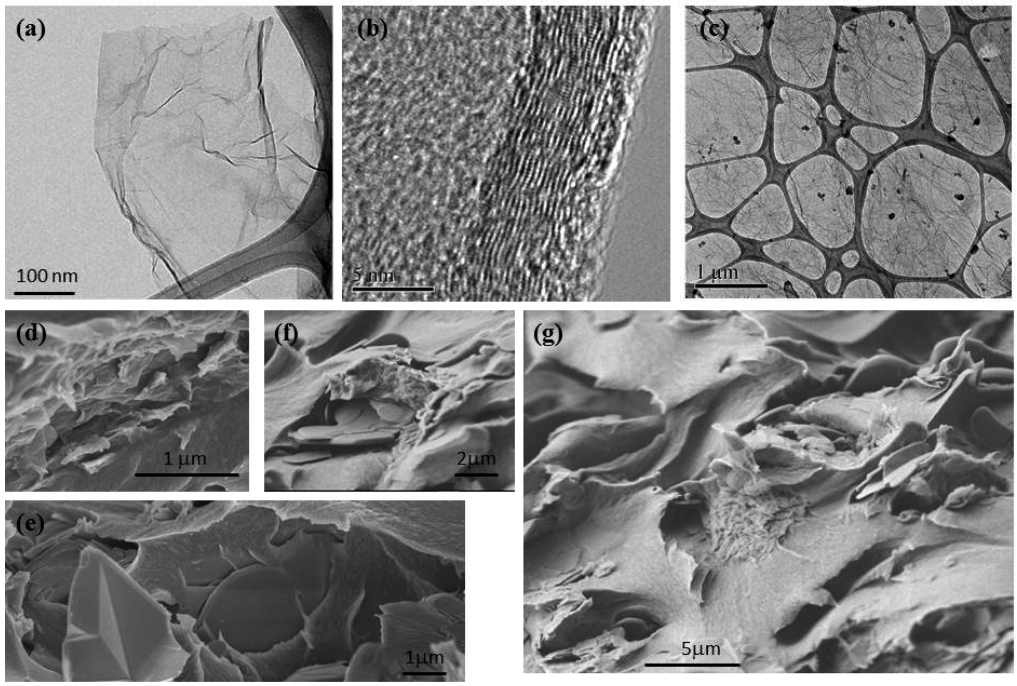

Figure 8. TEM images of (a, b) TrG and (c) g-TrG. SEM images of the fracture surface of (d) PI/g-TrG-1, (e) PI/f-BN-30, and (f, g) PI/f-BN-30/g-TrG-1.

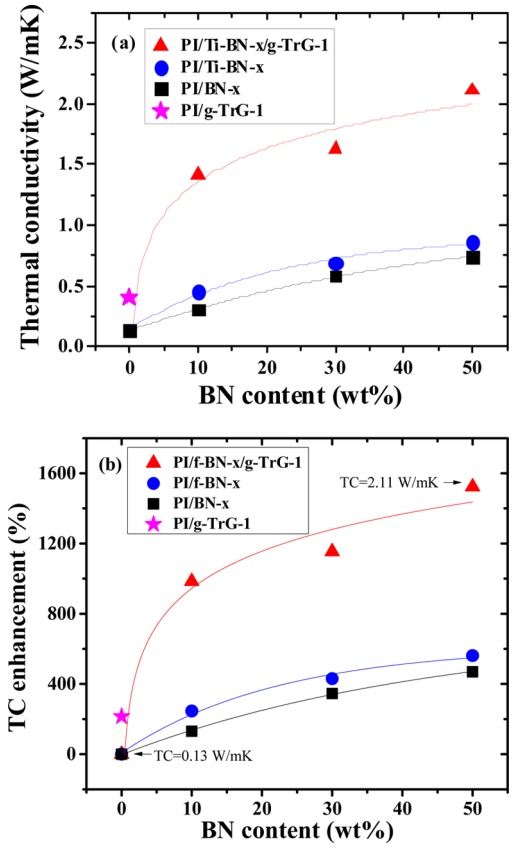

Figure 9. Effects of filler type and BN content on the (a) thermal conductivity (TC) and (b) TC enhancement of PI composites. The lines shown in both graphs represent the regression results.

2.11 W/mK. The enhancement in this TC value is as high as 1500% compared to the intrinsic PI film. The results indicate the efficient thermal conduction network is achieved by filling the silk-like g-TrG in the gap between f-BN and the PI matrix. Furthermore, the strong interactions between PI and all surface-modified fillers (f-BN and g-TrG) as illustrated in SEM images contribute the effective phonon transfer in the PI matrix. Consequently, the TC value of PI/f-BN/g-TrG is improved as well as the following thermal and mechanical properties.

The dimensional stability is an important issue for PI films, because they are commonly laminated with other metals or ceramics for further thermal processing. The CTE value is indicative to the dimensional stability of PI films and is evaluated by TMA results within the temperature range of 100 to 200 °C. The effects of filler type and BN content on the CTE of PI composite films are shown in Figure 10. The CTE of the PI/BN film decreases linearly with the increasing BN content. The surface modification on BN leads to stronger interaction between 2 phases that the CTE of composites can be further reduced. The CTE of PI/f-BN-50 is as low as 12 ppm/K, which is even lower than that of copper. Based on knowledge from the manufacturer, a PI film with a CTE lower than 30 ppm/K shows the potential in

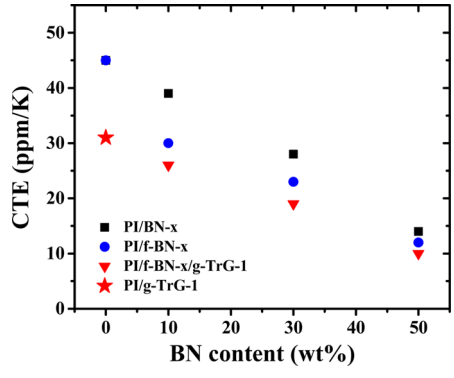

Figure 10. Effects of filler type and BN content on the coefficient of thermal expansion (CTE) of PI composites.

dx.doi.org/10.1021/am501323m | ACS Appl. Mater. Interfaces 2014, 6, 8639−8645

Table 1. Properties of PI and PI Hybrid Films[g]

	DMA			TMA	TGA		
sample	E′[a] (MPa)	Tg[b] (°C)	tan δ	CTE[c] (ppm/K)	Td_5[d] (°C)	TC[e] (W/mK)	Rs[f] (Ω)
pure PI	1515	415	0.25	45	550	0.13	$\sim10^{15}$
PI/f-BN-10	1726	419	0.24	30	576	0.45	$\sim10^{14}$
PI/f-BN-30	2775	411	0.22	23	584	0.69	$\sim10^{13}$
PI/f-BN-50	3901	398	0.18	12	590	0.86	$\sim10^{13}$
PI/g-TrG-0.1	2007	413	0.25	38	558	0.25	
PI/g-TrG-0.5	2443	416	0.24	32	570	0.33	
PI/g-TrG-1	2849	421	0.24	31	575	0.41	$\sim10^{13}$
PI/g-TrG-2	3060	427	0.25	29	582	0.52	
PI/f-BN-10/g-TrG-1	2119	419	0.23	26	567	1.41	$\sim10^{13}$
PI/f-BN-30/g-TrG-1	2913	414	0.20	19	576	1.63	$\sim10^{13}$
PI/f-BN-50/g-TrG-1	3805	403	0.16	10	591	2.11	$\sim10^{13}$

[a]Storage modulus at 60 °C. [b]The temperature at the maximum of tan δ curve is designated as Tg. [c]The coefficient of thermal expansion determined over the temperature range of 100−200 °C. [d]The thermal decomposition temperature at 5% weight loss. [e]The average thermal conductivity of at least 3 measurements of each sample. The percent error is 5 to 10%. [f]The average surface resistance of at least 3 measurements of each sample at room temperature. [g]f-BN: Ti-coupling agent-modified hybrid-sized hexagonal BN: 4 μm(30%) + 15 μm(70%).

practical FPC applications. Surprisingly, the reduction in CTE by g-TrG is more significant that the CTE of PI containing 1 wt % of g-TrG is 31 ppm/K, which is close to the value of PI/f-BN-10. The CTE lower than 30 ppm/K is obtained from PI composites containing more than 10 wt % of f-BN. The extent of reduction in CTE by additional 1 wt % g-TrG slightly decreases with the increasing BN contents. The micrometer-sized BN platelets predominantly improve the chain orientation of PI and thus suppress the thermal expansion of the PI matrix.[26,39−41]

Table 1 summarizes the thermal, mechanical, and electric properties of PI hybrid films. The surface resistance of each PI/f-BN/g-TrG film is checked to confirm the electrical insulating feature as substrates for electronic applications. The surface resistances of those PI/f-BN/g-TrG films are in the range of 10^{13} Ω indicating their sufficient electrical insulating property. The Tg value of PI films increases first when the loading of f-BN is 10 wt % and then decreases with the increasing f-BN contents. In contrast, the Tg value of PI films increases significantly with the increasing g-TrG amounts. The presence of g-TrG improves both the mechanical and thermal properties of PI films. The large f-BN platelets with functional groups on their edges lead to loosely packing of PI chains. Consequently, the weak chain−chain interaction results in a lower value of T_g. The rigidity of film is increased when the PI matrix containing BN platelets as shown by its tan δ (damping) lower than pure PI. On the other hand, the damping of PI/g-TrG is similar to that of pure PI. The rotational motion of PI main chains is effectively restricted by g-TrG that the Tg value of PI/g-TrG is higher than that of pure PI. The Tg value of PI containing 1 wt % of g-TrG is 421 °C. The Tg values of PI/f-BN/g-TrG are ranging from 403 to 419 °C, which are significantly higher than those of the PI/f-BN film. The increase in Tg value not only suggests a hindered rotation of PI chains by g-TrG but also an improved interfacial strength between phases. For pure PI, the thermal decomposition temperature T_d^5 is 550 °C. An increased T_d^5 value is observed for PI films containing either f-BN or g-TrG. The PI/f-BN/g-TrG hybrid films exhibit T_d^5 values in the range of 567 to 591 °C. Those thermally conductive fillers in PI films effectively dissipated heat from the PI matrix that improved the thermal stability of PI films. Notably, each PI film remains very flexible, even for the one containing 50 wt % of f-BN and 1 wt % of g-TrG, as illustrated in the digital photograph in Figure 1.

4. CONCLUSIONS

The combination of two types of thermally conductive and functionalized fillers f-BN and g-TrG in the PI matrix dramatically improves the TC and dimensional stability of PI films. The f-BN platelets significantly reduce the CTE of PI films, and, on the other hand, the silk-like g-TrG nanosheets complete the thermal conducting pathway throughout the PI/f-BN matrix by filling in the gaps. The thermal resistance at the interface between filler and PI is minimized due to the surface functional groups, and thus, the fillers serve as thermal interfacial materials to facilitate smooth heat transfer within polymer matrix. Furthermore, the thermally conductive PI/f-BN/g-TrG composites exhibit superior dimensional stability simultaneously. The flexible hybrid films have excellent mechanical strength and thermal stability for future substrate materials applied in the fields requiring efficient heat dissipation.

AUTHOR INFORMATION

Corresponding Author

*Phone: +886 4 24517250 ext. 3666. Fax: +886 4 24510890. E-mail: ihtseng@fcu.edu.tw.

Notes

The authors declare no competing financial interest.

ACKNOWLEDGMENTS

The authors would like to acknowledge the financial support from the Ministry of Economic Affairs, Taiwan, through the project on flexible polymeric materials for electronic application (100-EC-17-A-07-S1-120). We also acknowledge the support from the National Science Council of Taiwan under the grant number of NSC 100-2221-E-167-006.

REFERENCES

(1) Choi, M. C.; Kim, Y.; Ha, C. S. Polymers for Flexible Displays: From Material Selection to Device Applications. *Prog. Polym. Sci.* **2008**, *33*, 581−630.

(2) Wuu, D. S.; Chen, T. N.; Lay, E.; Liu, C. H.; Chang, C. H.; Wei, H. F.; Jiang, L. Y.; Lee, H. U.; Chang, Y. Y. Transparent Barrier Coatings on High Temperature Resisting Polymer Substrates for Flexible Electronic Applications. *J. Electrochem. Soc.* **2010**, *157*, C47−C51.

(3) Fukukawa, K.; Okazaki, M.; Sakata, Y.; Urakami, T.; Yamashita, W.; Tamai, S. Rational Approach for Improving Optical and Mechanical

Properties of Transparent Polyimide for FPC Substrate. *J. Photopolym. Sci. Technol.* **2011**, *24*, 255−258.
(4) Choi, M. C.; Hwang, J. C.; Kim, C.; Ando, S.; Ha, C. S. New Colorless Substrates Based on Polynorbornene-Chlorinated Polyimide Copolymers and Their Application for Flexible Displays. *J. Polym. Sci., Part A: Polym. Chem.* **2010**, *48*, 1806−1814.
(5) Lee, G. W.; Park, M.; Kim, J.; Lee, J. I.; Yoon, H. G. Enhanced Thermal Conductivity of Polymer Composites Filled with Hybrid Filler. *Composites, Part A* **2006**, *37*, 727−734.
(6) Xu, Y.; Chung, D. D. L.; Mroz, C. Thermally Conducting Aluminum Nitride Polymer-Matrix Composites. *Composites, Part A* **2001**, *32*, 1749−1757.
(7) Xie, S. H.; Zhu, B. K.; Li, J. B.; Wei, X. Z.; Xu, Z. K. Preparation and Properties of Polyimide/Aluminum Nitride Composites. *Polym. Test.* **2004**, *23*, 797−801.
(8) Hill, R. F.; Supancic, P. H. Thermal Conductivity of Platelet-Filled Polymer Composites. *J. Am. Ceram. Soc.* **2002**, *85*, 851−857.
(9) Sato, K.; Horibe, H.; Shirai, T.; Hotta, Y.; Nakano, H.; Nagai, H.; Mitsuishi, K.; Watari, K. Thermally Conductive Composite Films of Hexagonal Boron Nitride and Polyimide with Affinity-Enhanced Interfaces. *J. Mater. Chem.* **2010**, *20*, 2749−2752.
(10) Teng, C. C.; Ma, C. C. M.; Chiou, K. C.; Lee, T. M. Synergetic Effect of Thermal Conductive Properties of Epoxy Composites Containing Functionalized Multi-Walled Carbon Nanotubes and Aluminum Nitride. *Composites, Part B* **2012**, *43*, 265−271.
(11) Martin-Gallego, M.; Verdejo, R.; Khayet, M.; de Zarate, J. M. O.; Essalhi, M.; Lopez-Manchado, M. A. Thermal Conductivity of Carbon Nanotubes and Graphene in Epoxy Nanofluids and Nanocomposites. *Nanoscale. Res. Lett.* **2011**, *6*, 610−616.
(12) Li, T. L.; Hsu, S. L. C. Enhanced Thermal Conductivity of Polyimide Films via a Hybrid of Micro- and Nano-Sized Boron Nitride. *J. Phys. Chem. B* **2010**, *114*, 6825−6829.
(13) Kume, S.; Yamada, I.; Watari, K.; Harada, I.; Mitsuishi, K. High-Thermal-Conductivity AlN Filler for Polymer/Ceramics Composites. *J. Am. Ceram. Soc.* **2009**, *92*, S153−S156.
(14) Yang, S. Y.; Lin, W. N.; Huang, Y. L.; Tien, H. W.; Wang, J. Y.; Ma, C. C. M.; Li, S. M.; Wang, Y. S. Synergetic Effects of Graphene Platelets and Carbon Nanotubes on the Mechanical and Thermal Properties of Epoxy Composites. *Carbon* **2011**, *49*, 793−803.
(15) Teng, C. C.; Ma, C. C. M.; Chiou, K. C.; Lee, T. M.; Shih, Y. F. Synergetic Effect of Hybrid Boron Nitride and Multi-Walled Carbon Nanotubes on the Thermal Conductivity of Epoxy Composites. *Mater. Chem. Phys.* **2011**, *126*, 722−728.
(16) Kizilkaya, C.; Mulazim, Y.; Kahraman, M. V.; Apohan, N. K.; Gungor, A. Synthesis and Characterization of Polyimide/Hexagonal Boron Nitride Composite. *J. Appl. Polym. Sci.* **2012**, *124*, 706−712.
(17) Zhi, C. Y.; Bando, Y.; Tang, C. C.; Golberg, D. Boron Nitride Nanotubes. *Mater. Sci. Eng., R* **2010**, *70*, 92−111.
(18) Baruch, A. E.; Bielenki, L.; Regev, O. Thermal Conductivity Improvement of Electrically Nonconducting Composite Materials. *Rev. Chem. Eng.* **2012**, *28*, 61−71.
(19) Zhi, C.; Bando, Y.; Terao, T.; Tang, C.; Kuwahawa, H.; Golberg, D. Towards Thermoconductive, Electrically Insulating Polymeric Composites with Boron Nitride Nanotubes as Fillers. *Adv. Funct. Mater.* **2009**, *19*, 1857−1862.
(20) Shahil, K. M. F.; Balandin, A. A. Graphene−Multilayer Graphene Nanocomposites as Highly Efficient Thermal Interface Materials. *Nano Lett.* **2012**, *12*, 861−867.
(21) Balandin, A. A.; Ghosh, S.; Bao, W. Z.; Calizo, I.; Teweldebrhan, D.; Miao, F.; Lau, C. N. Superior Thermal Conductivity of Single-Layer Graphene. *Nano Lett.* **2008**, *8*, 902−907.
(22) Wajid, A. S.; Das, S.; Irin, F.; Ahmed, H. S. T.; Shelburne, J. L.; Parviz, D.; Fullerton, R. J.; Jankowski, A. F.; Hedden, R. C.; Green, M. J. Polymer-Stabilized Graphene Dispersions at High Concentrations in Organic Solvents for Composite Production. *Carbon* **2012**, *50*, 526−34.
(23) Schwamb, T.; Burg, B. R.; Schirmer, N. C.; Poulikakos, D. An Electrical Method for the Measurement of the Thermal and Electrical Conductivity of Reduced Graphene Oxide Nanostructures. *Nanotechnology* **2009**, *20*, 405704.
(24) Liang, Q. Z.; Yao, X. X.; Wang, W.; Liu, Y.; Wong, C. P. A Three-Dimensional Vertically Aligned Functionalized Multilayer Graphene Architecture: An Approach for Graphene-Based Thermal Interfacial Materials. *ACS. Nano* **2011**, *5*, 2392−2401.
(25) Tseng, I. H.; Chiang, J. C.; Lin, H. C.; Tsai, M. H. Polyimide/Boron Nitride Nanocomposites. *Chemistry* **2012**, *70*, 31−38.
(26) Tseng, I. H.; Chiang, J. C.; Huang, S. L.; Tsai, M. H. Enhanced Thermal Conductivity of Polyimide Composites by Functionalized Graphene Oxide. *Polym. Int.* **2013**, *62*, 827−835.
(27) Kan, L. Y.; Xu, Z.; Gao, C. General Avenue to Individually Dispersed Graphene Oxide-Based Two-Dimensional Molecular Brushes by Free Radical Polymerization. *Macromolecules* **2011**, *44*, 444−452.
(28) Buha, J. Solar Absorption and Microstructure of C-doped and H-co-doped TiO2 Thin Films. *J. Phys. D: Appl. Phys.* **2012**, *45*, 385305−385319.
(29) Wang, Y.; Shi, Z. X.; Yin, J. Boron Nitride Nanosheets: Large-Scale Exfoliation in Methanesulfonic Acid and Their Composites with Polybenzimidazole. *J. Mater. Chem.* **2011**, *21*, 11371−11377.
(30) Dai, X. J.; Chen, Y.; Chen, Z.; Lamb, P. R.; Li, L. H.; Plessis, J.; McCulloch, D. G.; Wang, X. Controlled Surface Modification of Boron Nitride Nanotubes. *Nanotechnology* **2011**, *22*, 245301−245307.
(31) Wang, G. X.; Yang, J.; Park, J.; Gou, X. L.; Wang, B.; Liu, H.; Yao, J. Facile Synthesis and Characterization of Graphene Nanosheets. *J. Phys. Chem. C* **2008**, *112*, 8192−8195.
(32) Chen, D.; Zhu, H.; Liu, T. X. In Situ Thermal Preparation of Polyimide Nanocomposite Films Containing Functionalized Graphene Sheets. *ACS Appl. Mater. Interfaces* **2010**, *2*, 3702−3708.
(33) Luong, N. D.; Pahimanolis, N.; Hippi, U.; Korhonen, J. T.; Ruokolainen, J.; Johansson, L. S.; Nam, J. D.; Seppala, J. Graphene/Cellulose Nanocomposite Paper with High Electrical and Mechanical Performances. *J. Mater. Chem.* **2011**, *21*, 13991−13998.
(34) Kim, H. M.; Lee, J. K.; Lee, H. S. Transparent and High Gas Barrier Films Based on Poly(vinyl alcohol)/Graphene Oxide Composites. *Thin Solid Films* **2011**, *519*, 7766−7771.
(35) Wang, X.; Yang, H.; Song, L.; Hu, Y.; Xing, W.; Lu, H. Morphology, Mechanical and Thermal Properties of Graphene-Reinforced Poly(butylene succinate) Nanocomposites. *Compos. Sci. Technol.* **2011**, *72*, 1−6.
(36) Wang, J. Y.; Yang, S. Y.; Huang, Y. L.; Tien, H. W.; Chin, W. K.; Ma, C. C. M. Preparation and Properties of Graphene Oxide/Polyimide Composite Films with Low Dielectric Constant and Ultrahigh Strength via In Situ Polymerization. *J. Mater. Chem.* **2011**, *21*, 13569−13575.
(37) Yang, D.; Velamakanni, A.; Bozoklu, G.; Park, S.; Stoller, M.; Piner, R. D.; Stankovich, S.; Jung, I.; Field, D. A.; Ventrice, C. A.; Ruoff, R. S. Chemical Analysis of Graphene Oxide Films After Heat and Chemical Treatments by X-ray Photoelectron and Micro-Raman Spectroscopy. *Carbon* **2009**, *47*, 145−152.
(38) Teng, C. C.; Ma, C. C. M.; Lu, C. H.; Yang, S. Y.; Lee, S. H.; Hsiao, M. C.; Yen, M. Y.; Chiou, K. C.; Lee, T. M. Thermal Conductivity and Structure of Non-Covalent Functionalized Graphene/Epoxy Composites. *Carbon* **2011**, *49*, 5107−5116.
(39) Ebisawa, S.; Ishii, J.; Sato, M.; Vladimirov, L.; Hasegawa, M. Spontaneous Molecular Orientation of Polyimides Induced by Thermal Imidization (5). Effect of Ordered Structure Formation in Polyimide Precursors on CTE. *Eur. Polym. J.* **2010**, *46*, 283−97.
(40) Jin, H. S.; Chang, J. H.; Kim, J. C. Synthesis and Characterization of Colorless Polyimide Nanocomposite Films Containing Pendant Trifluoromethyl Groups. *Macromol. Res.* **2008**, *16*, 503−519.
(41) Koo, M.; Bae, J. S.; Shim, S. E.; Kim, D.; Nam, D. G.; Lee, J. W.; Yeum, J. H.; Oh, W. Thermo-Dependent Characteristics of Polyimide-Graphene Composites. *Colloid Polym. Sci.* **2011**, *289*, 1503−1509.